FIZIKA 9 (1977) Supplement 4, 671–706
(Proceedings of the Int. Symp. on Nuclear Collisions and
Their Microscopic Description, Bled, September 1977)

HIGH DENSITY NUCLEAR MACH SHOCK WAVES IN CENTRAL HIGH ENERGY HEAVY ION COLLISIONS[+]

Horst Stöcker[++], Jürgen F. Hofmann, Werner Scheid[+++], and
Walter Greiner

Institut für Theoretische Physik
der Johann Wolfgang Goethe Universität
Frankfurt am Main, Germany

Abstract: High Density Nuclear Mach Shock Waves (HDNMSW) occuring in central high energy heavy ion collisions (chehic) are up to now the only tool to produce and investigate bulks of highly excited and strongly compressed nuclear matter. Due to strong meson condensates, phase transitions of dense nuclear matter into density isomeric states (superdense nuclei) can be expected. We discuss the occurence of pion condensation in - and the influence of phase transitions on - relativistic nucleus nucleus collisions. Calculated pion multiplicities are presented as function of the bombarding energy for central collisions of various projectile - target combinations. A new effect expected in chehic is the "strong cooling" of the strongly compressed nuclear matter due to the occurence of deeply bound pionic states and due to a phase transition from baryon to quark matter. We calculate the propagation of HDNMSW in a relativistic dynamical model. The comparison of the calculated angular - and energy distributions for the emission of matter with recent experimental data seems to indicate a phase transition in nuclear matter at densities of about 3 ρ/ρ_0.

1. Introduction:

Early speculations on the existence of abnormal superdense nuclei[1,2,3,4] ("Density Isomers") have recently been studied by field theoretical model calculation,[5-16] which show that compressed nuclear matter ($\rho/\rho_0 \gtrsim 2$) due to meson

[+] Talk presented by H. Stöcker

condensation may become unstable. Then it may undergo a phase transition into a new form of matter with densities, binding energies and (Z/m)-ratios several times the nuclear groundstate values[1-4,7-16,18] (see Fig. 1). At even higher densities ($\rho/\rho_0 \approx 10$) phase transitions from baryon to quark matter can be discussed.[17]

Although the stability of superdense nuclei is questionable because of their high surface energies[18] there may exist at least metastable superdense nuclear states.[14] Up to now the only feasible way to produce bulks of strongly compressed nuclear matter consists in the formation of nuclear shock waves[14,19-31] which occur in head-on collisions of two nuclei, when their relative velocity exceeds the nuclear sound velocity ($c_s/c \approx 0.2$). The nucleon Pauli principle then forces their wavefunctions apart,[19] which can be interpreted phenomenologically as compression energy. At higher energies the hard core of the nucleon-nucleon potential, which may stem from the Pauli principle for quark matter, gives strong repulsion.

Contrary to sound waves in nuclear matter[32] nuclear shock waves are connected with strong, density dependent matter flows with flow velocity $v_f(\rho)$. The shock front propagates with shock velocity $v_s(\rho)$, also strongly dependent on the compression amplitude. Hence very nonlinear phenomena appear for very large amplitudes, both $v_s(\rho)$ and $v_f(\rho)$ tend to the velocity of light c, while for small perturbations they approach the linear limit for sound waves (see Figs. 2,3).

2. Pion Condensation and the Validity of Hydrodynamics

The formation of nuclear shock waves calls for the validity of hydrodynamical concepts, which means that fast thermalization (short mean free path or more precisely: short longitudinal momentum decay length) during high energy heavy ion collisions must occur. High relative momenta between two nuclei, signifying no overlap in phase space, as well as large longitudinal momentum decay length's calculated from the free n-n scattering cross sections were interpreted as decease for nuclear shock waves at bombarding

energies above one GeV per nucleon.[27] However, in the "formation flight" of ensembles of nucleons collective phenomena become important: Pionic waves, produced in inelastic n-n collisions by the creation and decay of nuclear isobars (nucleon resonances) in processes of the type $N+N \rightarrow N+N^{*} \rightarrow N+\pi+N \rightarrow N^{*}+N \rightarrow \ldots$ may lead to rapid randomization of longitudinal momentum and energy and thus to short mean free path and to the generation of shock waves.[20-28,30,31] Recent experiments[26,34-40] have shown, that the reaction products show high multiplicities and large transverse momentum transfer, thus indicating short longitudonal momentum decay length and only little transparency.

Another important process for randomization is the critical scattering of nucleons in the vicinity of a phase transition point.[15,31,33] This is analogous to the critical opalescence, which is e.g. characterized by the great enhancement of the scattering cross section of light near a liquid-gas phase transition or the critical scattering of neutrons in ferromagnets near the Curie point or - as the last example - by the critical scattering appearing in two colliding plasma beams when the drift velocity of the two plasmas exceeds a critical value. Then unstable plasmon modes appear, resulting in the growth of strong electric fields, greatly reducing the penetration depth of the two plasma beams in comparison with estimated values from simple two body n-n collisions.

Thus the vicinity of a phase transition point, as the onset of pion condensation, is expected to be marked by the occurence of critical nucleon scattering, i.e. a large enhancement (a factor 2 - 4)[33] of the density dependent n-n-cross section and a sudden reduction of the longitudinal momentum decay length. Theoretically the onset of pion condensation is often described as the decay of the Hartree-Fock groundstate into ordered zero frequency (zero energy) particle-hole excitations carrying pionic quantum numbers. In the new phase at high density the groundstate nuclear matter consists of nucleons forming a spin-isospin lattice[11]. This can phenomenologically be interpreted as a phase transition from the nuclear liquid to a nuclear spin - isospin - crystal.

The occurence of a pion condensate in high energy heavy ion collisions depends strongly on the question of temperature, finite size and time scale during such collisions;[15,31,33] The critical temperatures $T_c(\rho)$ above which the thermal excitations destroy the ordered spin - isospin lattice lie substantially above those expected in shock waves (see Fig.4).

As the condensate occurs at finite momentum $k_c \approx 2\, m_\pi$, the critical distance $R_c \sim k_c^{-1} \approx 1$ fm. Thus a dense system of dimension ≈ 2 fm could support a condensate.

The relaxation time of the pion condensate can be estimated from $\tau_{cond}^{-1} = \max |2\, \mathrm{Im}\, \omega|$, where ω is the complex zero of the pion propagator Δ_π in nuclear matter. This gives $\tau_{cond} \sim \tau_0 \cdot \Delta\tilde{\rho}$ with $\tau_0 = 10^{-23}$ sec and $\Delta\tilde{\rho} = (\rho - \rho_c)/\rho_0$. As the collision time is of the order of $5\tau_0$ and $\tau_{cond} \approx \tau_0$ the time scale is not too good. More detailed calculations were needed.

In the following we assume local equilibrium as a first approximation, so that hydrodynamical concepts can be used in our calculations. We have incorporated in our calculations:

1) relativistic dynamics
2) particle (π -, N^* -) production
3) finite geometry
4) interactions and correlations between nucleons

3. The Nuclear Equation of State

We use a phenomenological description of nuclear matter, where phase transitions can be described as secondary minima or bends respectively in the density - dependent binding energy per nucleon $E_c(\rho)$ (see Fig. 1). We treat the colliding nuclei as droplets of nuclear matter, neglecting quantum mechanical effects as pairing, shell corrections and surface - as well as Coulomb energies, which are of the order of a few MeV per nucleon, while we are dealing with bombarding energies in the 0.1 - 4.2 GeV/N range. Furthermore, as the de Broglie wave length at these high energies is small compared to the nuclear dimensions, classical calculations are justified. Substantially below about 100 MeV/N, these

approximations will become worse.

Basic for the nuclear equation of state is the rest energy per nucleon W (ρ, T) as function of density ρ and temperature T. It can be written as

$$W(\rho,T) = M_o c^2 + E_c(\rho) + \sum_{i=0}^{N} \left(E_{T_i}(\rho_i, T) + E_i\right)\cdot\lambda_i + E_\pi(\rho_\pi, \rho, T)$$

Here $M_o c^2$ is the rest mass of a free (unbound) nucleon, and $E_c(\rho, T=0)$ gives the binding (compression) energy per nucleon in cold (T=0) nuclear matter. $E_c(\rho)$ is practically unknown: Only $E_c(\rho=0)=0$ and $E_c(\rho_o) = -16$ MeV (groundstate nuclear matter) are fairly certain. (See Fig. 1a). At higher densities, the nucleon Pauli principle causes repulsion, so that $E_c(\rho)$ increases smoothly up to a possible critical point, where phase transitions may occur (See Fig. 1): a "soft" pion condensation[6] may be described by a bend in $E_c(\rho)$, while strong meson condensation will result in a strong secondary minimum in $E_c(\rho)$[7-14,16] with negative pressure $(p<0)$ at the phase transition region. The drastic consequences on the propagation of shock waves are discussed below. Also the co - existence of two phases with different energies at the same density is possible, which may lead to two different shock waves in the first and second phase. For our dynamical calculation we first use $E_c = K/(18\rho\rho_o)\cdot(\rho-\rho_o)^2$ from the extended liquid drop model.[19] $E_{T_i}(\rho_i,T) = \beta_i/2\ \rho_i^{-2/3} T^2$ with $\beta_i = \left(\frac{2}{3}\tau_i\pi\right)^{2/3} M_i c^2/(\hbar c)^2$ is the thermal energy of the i-th baryonic resonance phase, the first term of a free Fermi-gas expansion. This is valid in good approximation for T < 100 MeV.

M_i, $E_i \equiv (M_i - M_o)c^2$ and $\rho_i = \lambda_i \rho$ are the mass, exitation energy and baryon number rest density of the i-th baryonic resonance phase respectively, while the $\tau_i = (2I_i+1)\cdot(2J_i+1)/4$ are statistical factors and the $\lambda_i = \tau_i e^{-E_i/T}\cdot\left(\sum_{k=0}^{N}\tau_k e^{-E_k/T}\right)^{-1}$ give the exitation probabilities for the different resonances.

The pionic energy is given by $E_\pi = \lambda_\pi\cdot\left(m_\pi^{eff} c^2 + \frac{3}{2}T\right)$ where $m_\pi^{eff} c^2$ is the rest mass of the pion, which at high densities may become very small[5] compared to the free pion

rest mass $m_\pi c^2 \simeq 138$ MeV. This is similar to the "diving" of electrons in supercritical fields (we refer to the article of W. Greiner at this meeting). (See Fig. 5)

$\frac{3}{2}T$ is the thermal energy and

$$\lambda_\pi = 1 \cdot e^{-\frac{m_\pi}{T}} + 2\, e^{-\frac{2m_\pi}{T}} + 3\, e^{-\frac{3m_\pi}{T}} + \ldots \simeq \frac{e^{-\frac{m_\pi}{T}}}{(1 - e^{-\frac{m_\pi}{T}})^2}$$

is the probability for multiple pion production. The pions are treated here as an ideal gas. This should be a fair approximation at the high temperatures occuring in shock waves. The pressure $p = \rho^2 \partial W/\partial \rho \,|_{S=const}$ has to be evaluated at constant entropy, which yields[26,41]

$$p = p_c + p_T + p_\pi$$

$$p = K/(18\rho_0)\cdot(\rho^2 - \rho_0^2) + \tfrac{1}{3}\rho^{1/3} T \sum_{i=0}^{N} \left\{ \beta_i \int_0^T \lambda_i^{1/3}\, dT \right\} + \lambda_\pi \rho T$$

The curvature in the first minimum of $E_c(\rho)$ is connected with the nuclear compression constant (incompressibility):

$$K = 9\rho^2 \partial^2 W/\partial^2 \rho \;\Big|_{\rho=\rho_0,\, T=0,\, S=const.}$$

which is of the order of $K \approx 100 - 400$ MeV, which corresponds to a sound velocity in groundstate nuclear matter

$$c_s/c = (\partial p/\partial(W\cdot\rho))^{1/2} \;\Big|_{S=const.}$$

where $W_0 \equiv W(\rho_0, T=0) \simeq 923$ MeV is the nucleon's groundstate energy. We used in our calculations K=300 MeV ($c_s/c = 0.19$).

4. The Relativistic Shock Equations

We have to require the conservation of

a) baryon number-
b) momentum -
c) energy -

} flux density

This yields the following consistency condition for the state variables in the rest system of the "shocked" and undisturbed (groundstate) nuclear matter:[26]

$$W^2(\rho,T) - W_0^2 + p(\rho,T)\cdot\left(W(\rho,T)/\rho - W_0/\rho_0\right) = 0$$

This equation is called the relativistic shock equation[25,26], which for $W - W_0 \ll W_0$ becomes $2(W-W_0) + p(\rho^{-1} - \rho_0^{-1}) = 0$ i.e. the (non-relativistic) Rankine-Hugoniot equation[21,22]. The shock front velocity $v_s(\rho)$ and the velocity for matter flow $v_c(\rho)$

with respect to the undisturbed matter are then given by[26]

$$v_s/c = (p \cdot W \cdot \rho / ((W\rho - W_0\rho_0)(W_0\rho_0 + p)))^{1/2}$$
$$v_f/c = (p \cdot (\rho \cdot W - \rho_0 W_0) / (\rho \cdot W \cdot (p + \rho_0 W_0)))^{1/2} \qquad \text{(see Fig. 3)}$$

respectively. One recognizes that v_s and v_f are proportional to $p^{1/2}$ where the pressure $p \sim \frac{\partial W}{\partial \rho}$. So in the presence of a phase transition, where the pressure becomes negative during the collapse, the shock phenomena must vanish. (see Fig. 6) This is of great importance for the possible detection of a density isomer.[14]

The above equations have to be solved numerically. For a nucleon gas, excluding resonances, pions and their "cooling" effects[22,26,30], we can find an unique analytical relation between thermal energy and density in the compressed matter[26]

$$E_T = \{-B + (B^2 - 4AC)^{1/2}\} / (2A)$$

where

$$A = 1 + \alpha \quad , \quad B = (W_0 + E_c) \cdot (2 + \alpha) + p_c/\rho - \alpha \frac{\rho}{\rho_0} W_0$$
$$C = (W_0 + E_c)^2 - W_0^2 + W_0 p_c (\rho^{-1} - \rho_0^{-1}) + E_c \cdot p_c \rho^{-1}$$

and $p_T = \alpha \rho E_T$, which with $\alpha = 2/3$ is valid for as well ideal- and Fermi-gases. Now we have a connection between all state variables behind the shock front and the velocities with the density ρ.

5. A relativistic model for central collisions of equal nuclei

The rest densities ρ and temperatures T in the compression region of two equal, centrally colliding nuclei can be evaluated in the center of mass-system by assuming that the velocity field in the compression zone is small[26] (this is true near the collision axis even for very high bombarding energies[30]). Then the flow velocity of the "shocked" matter in the projectile and target nucleus is equal to the c.m. velocity of projectile and target. ($v_o = v_f$) (See Fig. 5)

In the laboratory system, the projectile velocity is

$$v_p = 2 v_f \cdot (1 + v_f^2)^{-1}$$

and therefor the kinetic lab energy is $E_{LAB}/n = ((1-v_p^2)^{-1/2} - 1)\cdot W_o$

As we know $v_f(\rho)$ from the numerical solution of the relativistic shock equations, we get a unique relation between ρ and E_{LAB}/n. The density as a function of the bombarding energy E_{LAB}/n is shown in Fig. 7 for various equations of state. Within this model we have calculated the mean pion multiplicities for central collisions as a function of the bombarding energy per nucleon[41] (see Fig. 8):

$$\langle n_\pi \rangle = (\lambda_\pi + \sum_{i>0}^{N} \lambda_i) \cdot 2A_p$$

For bombarding energies $E_{LAB}/n > 0.4$ GeV $\langle n_\pi \rangle$ can fairly well be fitted by a straight line:

$$\langle n_\pi \rangle = (0.17 \cdot E_{LAB}/n\,[\mathrm{GeV}] - 0.04) \cdot 2A_p$$

Clearly, the excitation of nuclear isobars and pions at high energies costs the system a lot of thermal energy. Fig. 9 shows the "cooling" of the compressed nuclear matter due to the increasing number of nuclear isobars taken into account.[26]

It has been shown[42] that an exponentially increasing resonance spectrum results in a maximal temperature $T_{Max} \approx m_\pi c^2$ which can not be exceeded in high energy n-n collisions, as the exitation energy is pumped into additional mass of heavy resonances. This behaviour may be changed drastically in central high energy heavy ion collisions[41]: (See Figs.5,10) The strong collective nuclear forces in highly dense nuclear matter may lead to strongly bound pionic states with very small effective masses ($m_\pi^{eff} << m_\pi$).

These small effective masses, which may result from the repulsive π-π self interaction, prevent the pions from diving into their own negative continuum (in contrast to electrons, which may dive in the presence of supercritical Coulomb fields (we refer to the talk of W. Greiner at this conference)).

Due to such strongly bound pionic states the temperature in central high energy heavy ion collisions will be reduced substantially at high densities ($\rho/\rho_0 \geq 2$): many pions can thermally be created in this strongly bound state with small effective mass, thus wasting a lot of the exitation energy of the system. This sudden reduction of the temperature above a theshold bombarding energy can experimentally be detected, as the evaporation spectra of the reaction products and the mean pion multiplicity strongly depend on the temperature of the compression zone.[41]

Also the pion production rate will be significantly changed: the direct production of free pions as calculated above will be reduced substantially, but two step processes, e.g. the exitation of pions from the low lying state into the continuum become very important[41]. The expansion of the compression zone after the reaction makes the production of free pions feasible, which have been created in a bound state, which however approaches the upper continuum for smaller densities. These processes may lead to a much smaller limiting temperature $T_{MAX} \sim m_\pi^{eff} c^2$ in central high energy heavy ion collisions than that occuring in single n-n-collisions[42]. The strong cooling can also be expected for baryon - quark - matter phase transitions[41] from a nucleus to a giant quark bag : as the internal energy is distributed over a three times larger number of degrees of freedon, the quark matter temperature will be 1/3 of the nucleons temperature.

6. Central High Energy Collision of Small Projectile and Heavy Target: A Relativistic Dynamical Model[43]

Our model describes phenomenologically the geometry and dynamical variables during a central high energy collision of a smaller projectile and a heavy target and yields the angular- and energy distribution of the reaction fragments. We carried out the calculations in the lab-frame (target at rest). There are mainly three different phases of evolution during such a collision[14,26] (see Fig. 11).

The diving phase: The kinematically contracted projectile enters the target, becomes highly compressed and excited. In the diving process a splashing wave should lead to backward emission of matter.
The penetrating stage: The projectile interpenetrates the target, pushing matter to the side; thus initiating the sidewards travelling strongly compressed Mach shock wave.
The evaporation phase: The projectile- and Mach shock matter leaves the residual target which now evaporates, while projectile and Mach shock explode because of their very high excitation energies which correspond to temperatures from 20 - 60 MeV. (See Fig. 12)

The explosion of the head shock wave which contains at the end of the collision more than double the nucleons of the incoming projectile, corresponds to the explosion of the nuclear fireball, which has recently been used to explain angular- and energy distributions in non-central high energy heavy ion collisions.[37]

It may also be possible, that the strongly compressed and highly excited projectile explodes inside the target during the interpenetrating stage. This will lead to superstars with enormous multiplicities. In this case the Mach angle will be washed out and can not be seen. This will be taken into account in a further calculation.

To restrict the number of degrees of freedom, we parametrize the compression zone by two paraboloids, $z = a_1 r^2 + z_1$, $z = a_2 r^2 + z_2$, which describe the shock front and the backside of the compression zone respectively. The undisturbed part of the target nucleus is described by the part of a spheroid of radius R up to the shock front (paraboloid 1), while the residual nucleus is described by a spheroid up to the backside of the compression zone

(paraboloid 2) with a drilled hole of radius R_p in it. The residual nucleus has not yet been incorporated in our present calculations. The projectile (head shock wave) is divided from the Mach shock zone by a third paraboloid $z = -a_1 r^2 + z_2$ (see Fig.11).

So the geometry of the system is determined by four variables: a_1, a_2, z_1, z_2.

The dynamical variables (energy density, momentum, pressure, temperature, density) are obtained by assuming homogeneous density-, velocity-, and temperature fields in each compression region. Thus for the sake of simplicity we concentrate on the mean values of the physical observables in the different regions as a function of time.

The shock equations yield an unique relation between energy, pressure, temperature, velocities, and the rest density in the compression zone. Using these, we can describe the stage of our system by the four geometrical variables and the density in the Mach- and head shock region.

To describe the evolution of the system in time, we need six differential equations for these six variables:

The surface points on the paraboloids shall fulfil the shock equations. They move with the shock velocities:

$$\frac{dF}{dt} = \frac{\partial F}{\partial t} + \vec{\nabla}\cdot\vec{F} = 0 \quad \curvearrowright \quad \dot{z}_1 = v_s(\rho_1)\,, \quad \dot{z}_2 = v_f(\rho_1)$$

$$\dot{a}_1 = \left(v_s(\rho_2)\cdot\left(1 + 4a_1^2 r_{p_1}^2\right)^{1/2} - v_s(\rho_1)\right)\cdot r_{p_1}^{-2}$$

$$\dot{a}_2 = \left(v_f(\rho_2)\cdot\left(1 + 4a_2^2 r_{p_2}^2\right)^{1/2} - v_f(\rho_2)\right) : r_{p_2}^{-2}$$

where F is the surface.

The time derivatives of the Mach- and head shock densities are determined by use of the conservation of the total baryon number A_G and the total energy E_G

a) $$A_G = A_T + A_p = \int_{V'} \rho'(x)\, d^3x$$

b) $$E_G = (A_T + A_p)\cdot W_0 + E_{LAB}\cdot A_p = \int_{V'} \rho'(x)\, W'(\rho'(x), T(\rho'(x)))\, d^3x = \sum_j \rho_j' W_j' V_j'$$

There j indicates the different density regions. The primes indicate the quantities in the lab frame. They are connected by Lorentz-transformations with the quantities in the respective rest frame:

$$\rho'(x) = \rho(x)\cdot (1 - v_f^2(\rho(x)))^{-\frac{1}{2}}\,, \quad W' = W\cdot (1 - v_f^2)^{-\frac{1}{2}}$$

The indices 0, 1, 2 are connected with the rest target, head- and Mach shock respectively. The differentiation of a) and b) with respect to time yields:

a') $$\frac{d}{dt}\rho_2' = -\left\{ \left(\rho_0' \frac{dV_0'}{dt} + \frac{d\rho_1'}{dt} V_1' + \rho_1' \frac{dV_1'}{dt} \right) V_2' + \frac{dV_2'}{dt} \left(A_T + A_p - \rho_0' V_0' - \rho_1' V_1' \right) \right\} \cdot V_2'^{-2}$$

b') $$\frac{d}{dt}\rho_1' = -\left\{ \sum_{j=0}^{2} \rho_j' \frac{dV_j'}{dt} \cdot \left(W_j' - W_2' - \rho_2' \frac{\partial W_2'}{\partial \rho_2'} \right) \right\} \cdot \left\{ V_1' \left(W_1' + \rho_1' \frac{\partial W_1'}{\partial \rho_1'} - \left(W_2' + \rho_2' \frac{\partial W_2'}{\partial \rho_2'} \right) \right) \right\}^{-1}$$

where $$\frac{\partial W_j'}{\partial \rho_j'} = \left\{ \frac{\partial W_j}{\partial \rho_j} \cdot \gamma_j + W_j \frac{\partial \gamma_j}{\partial \rho_j} \right\} \cdot \left\{ \gamma_j + \rho_j \frac{\partial \gamma_j}{\partial \rho_j} \right\}^{-1}$$

with $$\gamma_j = (1 - v_f^2(\rho_j))^{-1/2}$$

and $$V_j' = \int_{z_j} r^2(z)\, dz$$

The V_γ' are calculated using the rotational symmetry around the z-axis. The time derivatives of V_γ' depend on the geometrical parameters and their time derivatives only. The quantities ρ_j, W_j, v_{fj} in the rest system are calculated by numerical interation from the primed lab-quantities. Also the initial values of the densities, velocities, and geometrical parameters are iteratively calculated by requiring the correct total energy and baryon number.

The time evolution of the physical quantities is obtained by simultaneous numerical integration of the six differential equations in time-steps of $\Delta t = 0.1$ fm/c, which is sufficiently exact to ensure energy- and baryon - number conservation better than one per cent.

7. The Results of the Calculations

The head- and the Mach shock densities ρ_1 and ρ_2 as a function of time are shown in Fig.13 for various energies: In the beginning, the projectile is strongly compressed, but this compression is substantially decreased later on. The Mach shock density ρ_2 is about 2 ρ_0 below ρ_1 respectively.

The mean compression in the head- and Mach shock (each at t = 5 fm/c) is shown in Fig.14a as function of the bombarding energy. The mean kinetic energy $E_{KIN}=((1-v_f^2)^{-1/2}-1)\cdot W_0$ of the emitted particles (Fig.14b) after the collision is smaller than 200 MeV/N for Mach shock particles up to bombarding energies of 5 GeV/N, while it is larger than this experimentally important threshold for the projectile (head shock) at high energies. The temperature in head- and Mach shock just after the collision is shown in Fig.14c. It has been corrected within our one-dimensional model of chapter 5 by the cooling influence of nuclear isobars which

were not yet included in our present calculations.

As the mean head shock densities are approximately equal to those calculated within the one-dimensional model[26], we can make use of the later model to yield the pion production rate, when we take care of the result, that the number of headshock particles is about $2A_p$.

The Mach shock angle φ is depicted as a function of lab-energy in Fig. 15. It smoothly decreases from about 60 degrees at 0.1 GeV/N to 35 degrees at 4 GeV/N. It is smeared out very much because of the temperature in the Mach shock and because of the curvature of the Mach-"cone".[26] The explosion of the highly excited head shock causes strong emission of fast particles into forward directions, which may hinder the visibility of the Mach shock peak at small bombarding energies. The energy spectra of the exploding projectiles (head shock) drawn in Fig.16 were calculated by relativistic addition of the flow velocity and the thermal velocity in the head shock after the collision, taking into account the isotropic decay cross section in the rest system of the projectile.

8. The Influence of a Density Isomer on the Reactions

If we assume a density isomer at $\rho/\rho_0 \approx 3$, the above picture applies only below E_{LAB} 0.2 GeV/n, as then the projectile density reaches the phase transition region, i.e. the region of negative pressure ($p < 0$) (see Figs. 1,6,15,17,18). The projectile collapses into the density isomeric state. Thus the quasi-stable nuclear crystal can move with rather small dispersion through the surrounding normal nuclear fluid. One may think on a piece of ice which moves through water - this is important for the appearance of the Mach shock wave, since a water droplet dumping into water would produce too high friction

and therefore soon damp out the collective motion. This, in fact, can to some extent be seen in the hydrodynamic calculations of Nix et al.[29]

As during the phase transition the head shock velocity becomes small, the Mach shock angle φ substantially decreases in this energy region, since the Mach shock moves faster than the collapsing head shock during this time period. The crystallization of the projectile causes a much more pronounced Mach shock peak at higher energy, because the projectile moves with much less friction through the target.

At bombarding energies of about 1.5 GeV/n the Mach shock density approaches the critical region: Now the Mach shock matter collapses into the density isomeric state and the Mach shock velocity becomes small, so that the Mach angle now will be substantially increased. (See Figs. 15 and 17)

It will also be broadened out due to the rapid change in Mach shock velocity within a small density regime. At even higher bombarding energies, the Mach angle shall decrease again as both v_{HS} and v_{MS} tend to the light velocity c at very high densities, so that $\varphi \to 0$ for very high energies.

One also may think that higher phase transitions do occur, which may again produce such a characteristic dependance of the Mach angle φ on the bombarding energy.

9. Comparison of Our Calculations with the Experimental Observations

HDNMSW should be observable in central high energy collisions of light projectiles with heavy

targets:

1) In azimuthally symmetric central collisions, which can be identified by very high multiplicities and azimuthally symmetric distributions of the reaction fragments e.g. by many prong stars in AgCl - detectors, a preferential emission angle must be observed[26].

2) The kinetic energy of these particles will be smaller than 200 MeV/N. It may be decreased to even lower values, if the Mach shock density is in the secondary minimum.

3) The Mach shock peak and the decay of the head shock should predominantly be seen in the α-particle channel for three reasons:
   a) A pion condensate with a structure of a spin-isospin lattice preferentially decays into α-particles as smallest lattice cells.
   b) When the Mach shock wave approaches the nuclear suface, it kicks out the α-particles contained enhanced in the nuclear surface.
   c) During the individual collisions of the constituent particles in the high temperature zone of the Mach shock, mainly those α-particles (and heavier clusters) survive, which have not undergone a scattering. Thus the Mach angle is conserved by those clusters, while scattered and unscattered nucleons cannot be distinguished.

4) One should find fast pions emitted by highly excited nuclear matter . The occurence of pion condensation should also lead to a large enhancement of the pion production cross section.

5) Simultaneously to the medium energy sidewards Mach shock peak, a broad high energetic forward peak at $\varphi \approx 40^{\circ}$, stemming from the exploding head shock, will be seen. It may consist of protons and pions mainly because of the extremly high temperatures in the head shock. Evidence for this projectile explosion seems to be seen in a recent experiment[44]. (See Figs. 12 and 19)

6) A nearly isotropic distribution in the lab frame may stem from the residual nucleus with small temperatures and kinetic energies.

In the presence of a pion condensate the Mach shock peak should be more clearly pronounced and also should have the above predicted dependence on energy. Recent experimental data,[26,36,38-40] which fulfil the above criteria on centrality, energy- and α-particle windows, show a peak in the angular distributions of the reaction fragments. The systematic shift of this preferential angle with energy can be interpreted in comparison with our calculations as indication for a phase transition in dense nuclear matter at $\rho/\rho_0 \approx 3\text{-}5$ (see Figs. 15 and 20, and figure caption).

10. Summary and Conclusions

HDNMSW can be used as a tool to study bulks of highly excited and strongly compressed nuclear matter, which means the investigation of the nuclear equation of state under extreme conditions. We have shown, that HDNMSW show specific effects, when phase transitions of nuclear matter into the pion condensate or density isomer occur at high densities. We can study the properties of the so-formed highly excited isobaric gas (eventually quark gas), and we can look for a possible limiting temperature T_{MAX} which may be drastically decreased by the strong cooling due to strongly bound pionic

states or a baryon-quark matter phase transition.

Besides that, information on the compressibility constant K and sound velocity c_s in ground state nuclear matter can be gained. It thus seems that high energy heavy ion physics can furnish fundamental information about nuclear matter. This may lead to an exciting future.

References

+ This work has been supported by the Bundesministerium für Forschung und Technologie (BMFT) and by the Gesellschaft für Schwerionenforschung (GSI).

+++ Permanent address: Institut für Theoretische Physik, Justis Liebig Universität, Gießen, Germany.

1) E. Feenberg and H. Primakoff, Phys. Rev. 70 (1946) 980

2) A. R. Bodmer, Phys. Rev. D 4 (1971) 1601

3) A. R. Bodmer, in Proceedings of the International Symposium on Present Status and Novel Developments in the Nuclear Many-Body Problem, Rome, Italy, 1972, edited by F. Calogero and C. Ciofi Degli Atti (Editrice Compositori, Bologna, 1973), Vol. 2, p. 505

4) Y. Ne'eman, in Proceedings of the International Astronomical Union Symposium No. 53 on Physics of Dense Matter, Boulder, Colorado, 1972, edited by C. J. Hansen (Reidel, Dordrecht/Boston, 1974), p. 111

5) A. B. Migdal, Zh. Eksp. Teor. Fiz. 61 (1971) 2209

6) R. F. Sawyer and D. J. Scalapino, Phys. Rev. D 7 (1973) 953;
W. Weise and G. E. Brown, Phys. Lett. 48B (1974) 297;
G. Baym and E. Flowers, Nucl. Phys. A222 (1974) 29

7) T. D. Lee and G. C. Wick, Phys. Rev. D 9 (1974) 2291

8) T. D. Lee, Rev. Mod. Phys. 47 (1975) 267

9) A. K. Kerman and L. D. Miller, in Proceedings of the 2nd High Energy Heavy Ion Summer Study, Berkeley, California, 1974, edited by L. S. Schroeder (Lawrence Berkeley Laboratory Report No. LBL-3675, 1975 (unpublished)), p. 73

10) E. M. Nyman and M. Rho, Nucl. Phys. A268 (1976) 408

11) J. M. Irvine, Rep. Prog. Phys. 38 (1975) 1385

12) D. K. Campbell, R. F. Dashen, and J. T. Manassah, Phys. Rev. D 12 (1975) 979

13) D. K. Campbell, R. F. Dashen, and J. T. Manassah, Phys. Rev. D 12 (1975) 1010

14) J. Hofmann, H. Stöcker, U. Heinz, W. Scheid, and W. Greiner, Phys. Rev. Lett. 36 (1976) 88

15) V. Ruck, M. Gyulassy, and W. Greiner, Z. Phys. A277 (1976) 391

16) A. B. Migdal, G. A. Sorokin, O. A. Markin, and I. N. Mishustin, Phys. Lett. 65B (1976) 423

17) F. Iachello, W. D. Langer, A. Lande, Nucl. Phys. A219 (1974) 612 ;
G. Chapline and M. Nauenberg, preprint, Lawrence Livermore Lab. (1976)

18) U. Heinz, H. Stock, W. Scheid, and W. Greiner, J. Phys. G (Nucl. Phys.) 3 (1977) 21

19) W. Scheid, R. Ligensa, and W. Greiner, Phys. Rev. Lett. 21 (1968) 1479

20) G. F. Chapline, M. H. Johnson, E. Teller, and M. S. Weiss, Phys. Rev. D 8 (1973) 4302

21) W. Scheid, H. Müller, and W. Greiner, Phys. Rev. Lett. 32 (1974) 741

22) W. Scheid, J. Hofmann, and W. Greiner, in Proceedings of the 2nd High Energy Heavy Ion Summer Study, Berkeley, California, 1974, edited by L. S. Schroeder (Lawrence Berkeley Laboratory Report No. LBL-3675, 1975 (unpublished)), p. 1

23) G. F. Chapline, in Proceedings of the 2nd High Energy Heavy Ion Summer Study, Berkeley, California, 1974, edited by L. S. Schroeder (Lawrence Berceley Laboratory Report No. LBL-3675, 1975 (unpublished)), p. 51

24) C. Y. Wong and T. A. Welton, Phys. Lett. 49B (1974) 243

25) J. Hofmann, H. Stöcker, W. Scheid, and W. Greiner, in Proceedings of the Bear Mountain Symposium on Relativistic Heavy Ions (1974)

26) H. G. Baumgardt, J. U. Schott, Y. Sakamoto, E. Schopper, H. Stöcker, J. Hofmann, W. Scheid, and W. Greiner, Z. Phys. A273 (1975) 359
H. Stöcker, Diploma Thesis, Frankfurt 1975 (unpublished)

27) M. I. Sobel, P. J. Siemens, J. P. Bondorf, and H. A. Bethe, Nucl. Phys. A251 (1975) 502

28) Y. Kitazoe, M. Sano, and H. Toki, Nuovo Cimento Lett. 13 (1975) 139

29) A. A. Amsden, G. F. Bertsch, F. H. Harlow, and J. R. Nix, Phys. Rev. Lett. 35 (1975) 905

30 J. Hofmann, W. Scheid, and W. Greiner, Nuov. Cim. 33A (1976) 343

31) J. Hofmann, H. Stöcker, M. Gyulassy, W. Scheid, and W. Greiner, Proceedings of the International Conference on Selected Topics in Nuclear Structure Dubna

32) A. E. Glassgold, W. Heckrotte, and K. M. Watson, Ann. Phys. (N.Y.) 6 (1959) 1

33) M. Gyulassy and W. Greiner, to be published in Ann. Phys.

34) B. Jakobsson, R. Kullberg, and I. Otterlund, Z. Phys. A272 (1975) 159

35) A. M. Poskanzer, R. G. Sextro, A.M. Zebelman, H. H. Gutbrod, A. Sandoval, and R. Stock, Phys. Rev. Lett. 35 (1975) 1701

36) H. G. Baumgardt, E. Schopper, J. U. Schott, N. P. Kocherov, A. V. Voronow, I. D. Issinsky, and L. G. Makarov, in Proceedings of the International Workshop IV on Gross Properties of Nuclei and Nuclear Excitations, Hirschegg, Kleinwalsertal, Austria, 1976 (Technische Hochschule Darmstadt Report No. AED-Conf. 76-015-000, 1976 (unpublished), p. 105

37) G. D. Westfall, J. Gosset, P. J. Johansen, A. M. Poskanzer, W. G. Meyer, H. H. Gutbrod, A. Sandoval, and R. Stock, Phys. Rev. Lett., 37 (1976) 1202

38) H. Heckman, private communication

39) I. Otterlund, private communication

40) E. Schopper, H. G. Baumgardt, J. U. Schott, to be published

41) H. Stöcker, W. Scheid, and W. Greiner, to be published

42) R. Hagedorn, Supp. Nuovo Cim. III. 2 (1965) 147

43) H. Stöcker, W. Scheid, and W. Greiner, to be published

44) S. Nagamiya et. al., LBL-preprint, 1977

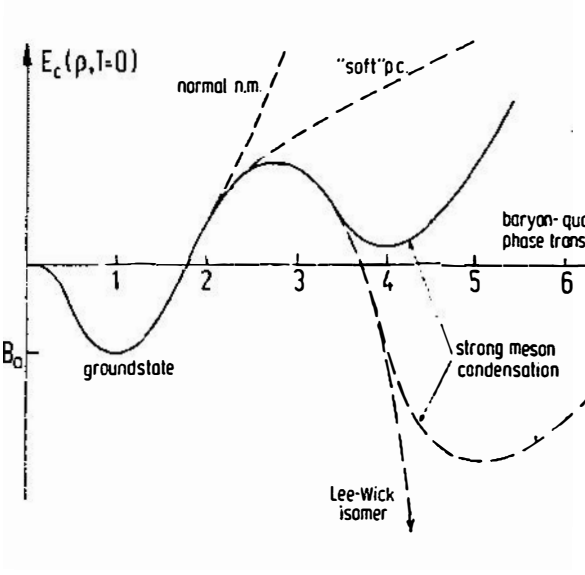

Fig. 1: shows various possible forms of the binding energy $E_c(\rho)$ per nucleon (as described in the text).

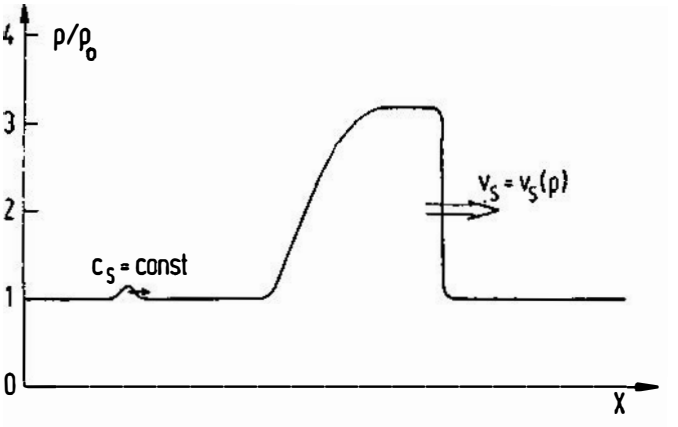

Fig. 2: shows schematically the difference between weak and strong compression waves (sound- and shock waves)

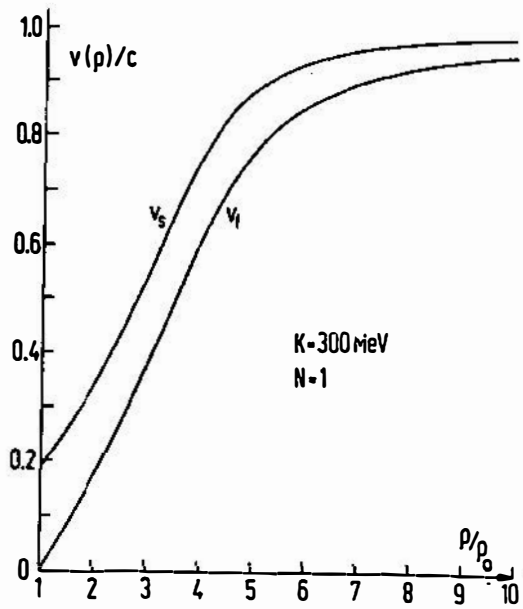

Fig. 3.

shows the strong dependence of the shock velocities on the compression amplitude [26].

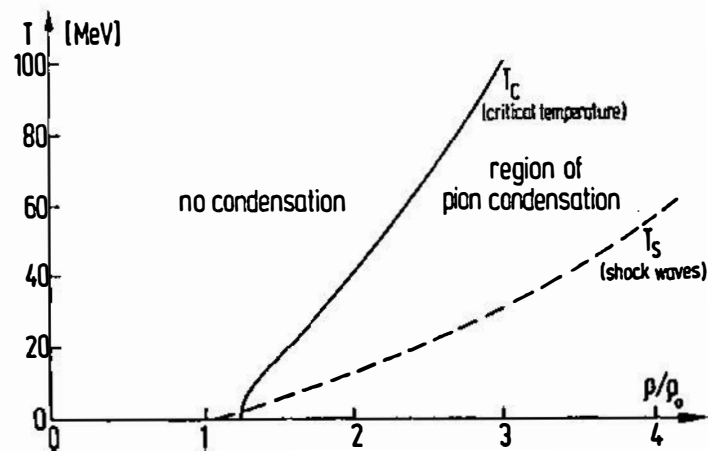

Fig. 4: Phase diagram of nuclear matter, which shows, that the critical temperature T_c (ρ) above which a possible pion condensate cannot be formed, is always much higher than the temperature occuring in nuclear shock waves. So pion condensates can occur in high energy heavy ion collisions.[15]

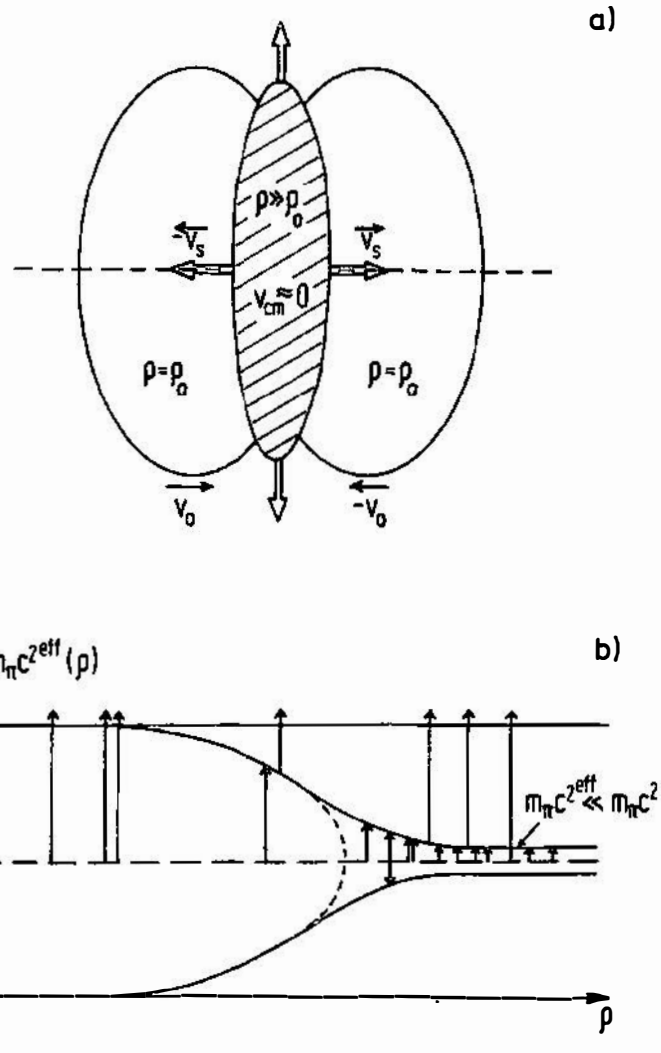

Fig. 5a: A head-on collision of two equal relativistically contracted nuclei is shown schematically.

b: The occurence of a strongly bound pionic state in high density nuclear matter is indicated schematically. The thermal production of pions is indicated by arrows for direct - and two step processes.

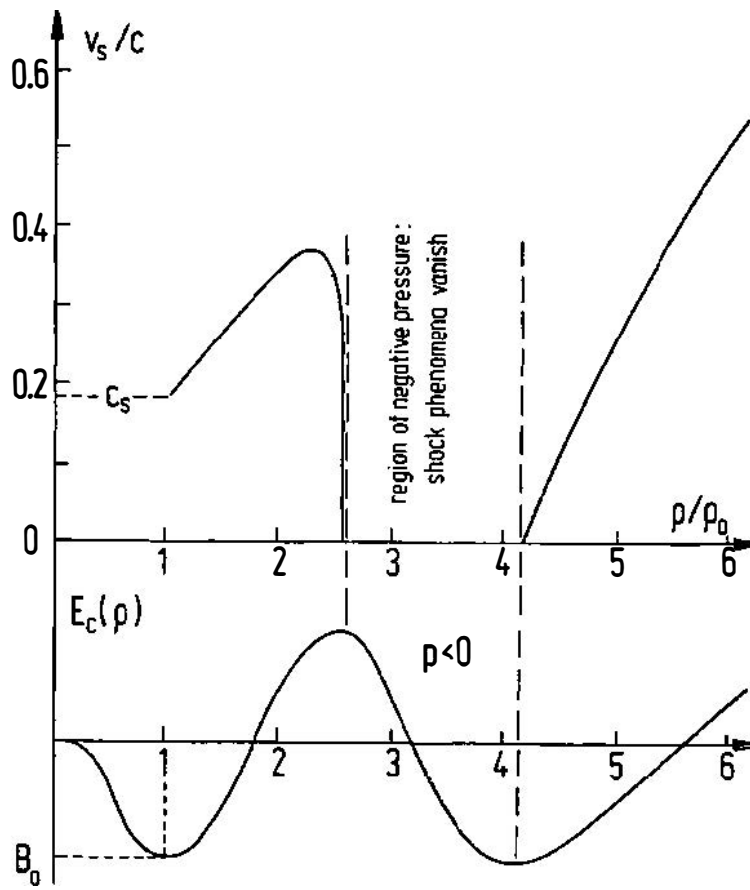

Pig. 6: The influence of a secondary minimum in $E_c(\rho)$ on the propagation of shock waves is shown[16]: in the region of negative pressure ($p < 0$) the shock phenomena vanish.

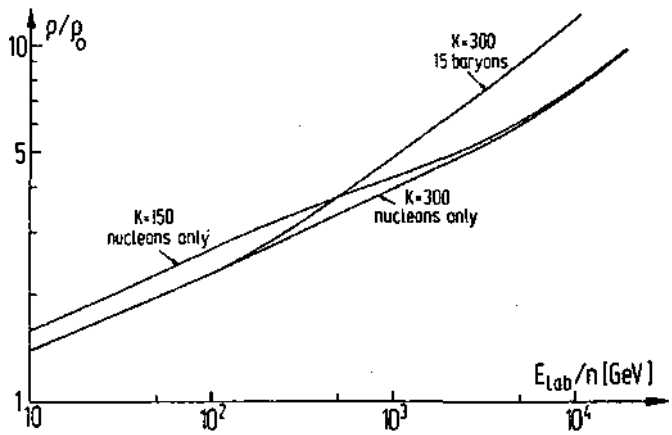

Fig. 7. The influence of the compression constant and excitation of nuclear resonances on the compression achievable in central collisions of two equal nuclei is shown[26]. The compression constant is of (rather small) importance for small bombarding energies (below 1 GeV/n), while isobars and pion production become very important for high bombarding energies (above 0.5 GeV/n).

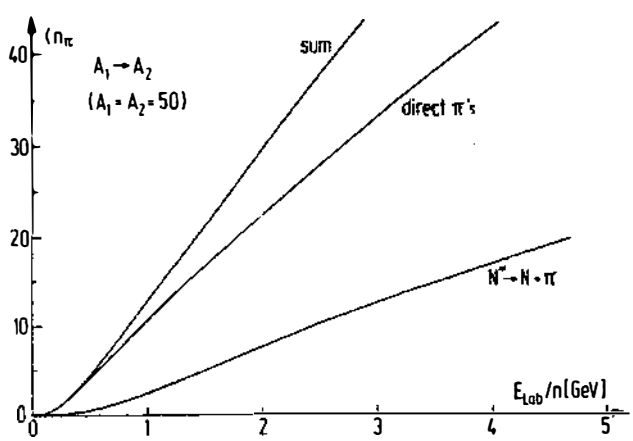

Fig. 8. The mean pion multiplicity $\langle n_\pi \rangle$ as function of the bombarding energy is depicted. Most pions stem from the direct thermal production of free pions, but a considerable part stems from the decay of thermaly excited nuclear isobars. The number of pions emitted from central high energy heavy ion collisions thus can be used to measure the temperature T achieved in the reaction.

$\langle n_\pi \rangle$ can also be used to determine the compressibility of nuclear matter: For a low compression constant (K = 100 MeV) the number of emitted pions at 1 GeV/n will be about 30 percent larger than for K = 300 MeV [26,41].

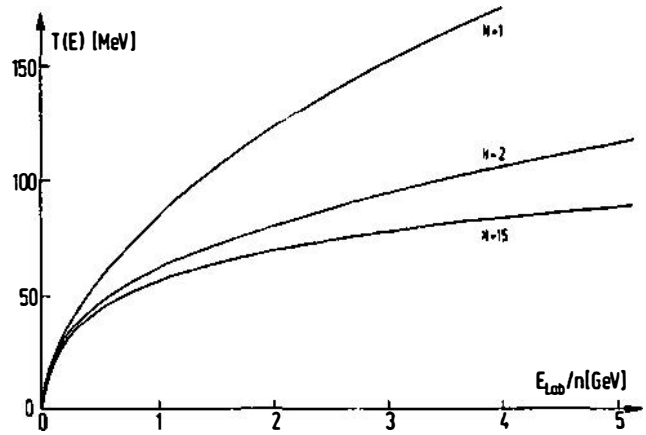

Fig. 9. The lowering of the temperature due to the exitation of resonances is shown: If the number of resonances taken into account in our calculation is increased, the temperature is substantially decreased as a function of bombarding energy. This shows the trend to a limiting temperature $T_{MAX} \approx m_\pi c^2$ at very large energies for an exponentially increasing resonance mass spectrum [42].

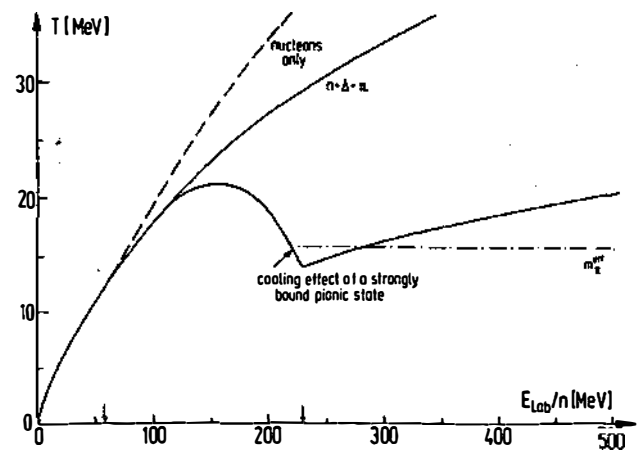

Fig. 10. The strong cooling of the reaction zone in the presence of a strongly bound pionic state ($m_\pi^{eff} c^2 \approx 16$ MeV at $\rho/\rho_0 > 3$) is depicted. Two step processes[41] will lower the temperature even more for very high temperatures.

Due to these strong collective effects in bulks of highly compressed nuclear matter the maximal temperature T_{MAX} will be drastically decreased in comparison with the maximal temperature $T_{MAX} \approx m_\pi c^2$ possibly occuring in single nucleon - nucleon collisions.

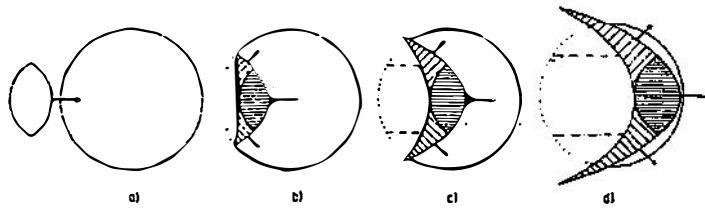

Fig. 11: shows the various stages of a head-on collision of a 720 MeV/n ^{16}O-nucleus with a ^{238}U-nucleus (which is at rest in the laboratory frame), calculated within our relativistic dynamical model.

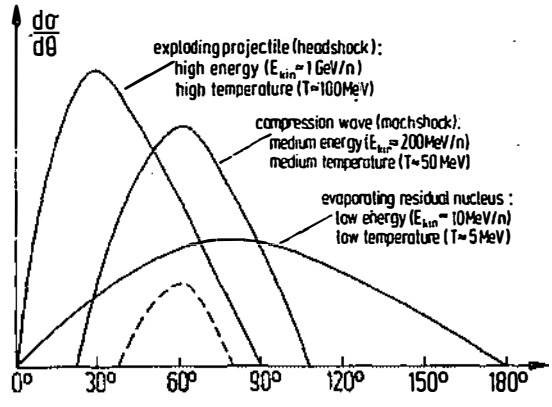

Fig. 12. The angular distribution of the reaction fragments in cluLic is shown schematically to consist of three different parts:

a) the high energy broad forward peak, stemming from the exploding projectile

b) the mean energy sidewards peak, stemming from the matter contained in the Mach shock wave.

c) the low energy isotropic background stemming from the evaporation of the residual nucleus.

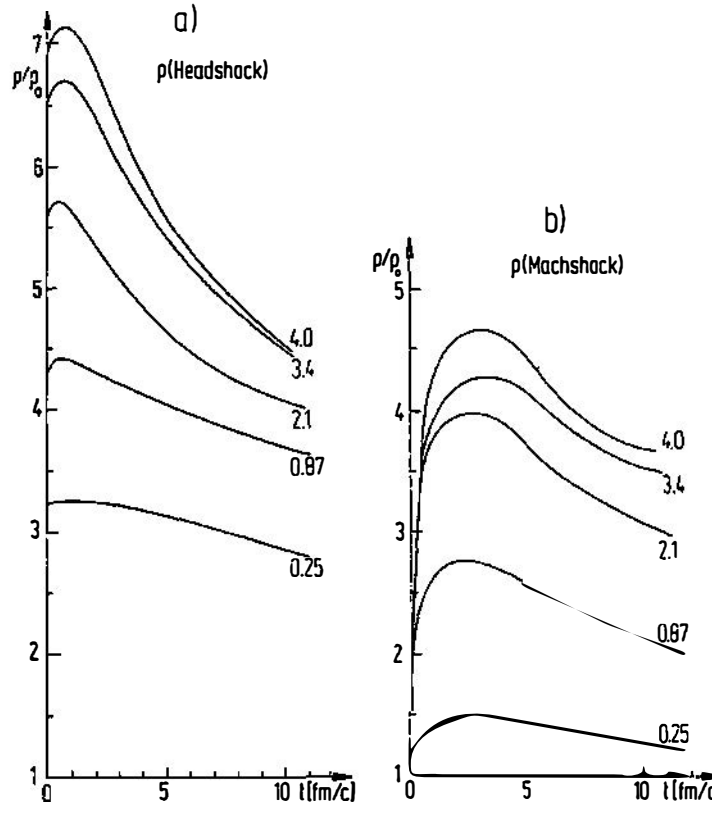

Fig. 13: show the head- and Mach shock densities as a function of time for various bombarding energies. The numbers at the curves indicate the bombarding energy in GeV/n.

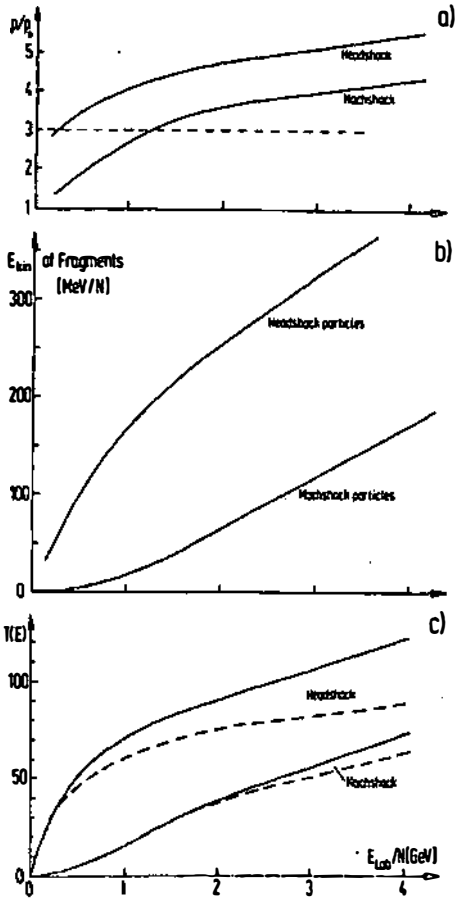

Fig. 14.a The mean density of the head- and the Mach shock (at t = 5 fm/c respectively) as function of the bombarding energy is depicted. An indicated phase transition at a given density will affect the headshock formation for relatively low energies, while the Mach shock will reach this phase transition region at much higher energies.

Fig. 14.b The kinetic energy E_{kin} per nucleon of the reaction fragments stemming from the head- and Mach shock respectively is drawn as a function of the bombarding energy. (The thermal energy is not yet included.)

Fig. 14.c The temperatures of the head- and Mach shock before their explosion is shown. The dashed lines are the temperatures taking into account the cooling influence of the production of nuclear isobars.

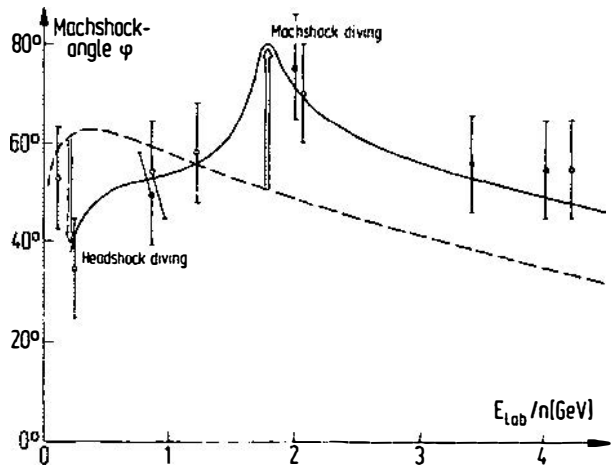

Fig. 15: The dashed line shows the energy dependent position of the Mach shock peak calculated without a density isomer in E_c (ρ). The solid line shows the influence of a phase transition point at $\rho/\rho_0 \approx 3$: At 0.25 GeV/N the projectile dives into the density isomeric state (crystallization) which results in a smaller angle than expected without density isomer. At energies between 1 and 2 GeV, the Mach shock reaches the phase transition region, resulting in a larger Mach shock angle ($\varphi \to 90^\circ$). It tends to smaller angles for even higher energies. The dots represent the peak position in recent experiments of E. Schopper and collaborators. They show just the behaviour which can be expected within our model. This seems to indicate the existence of a phase transition (secondary minimum) in nuclear matter at about $3\rho/\rho_0$.

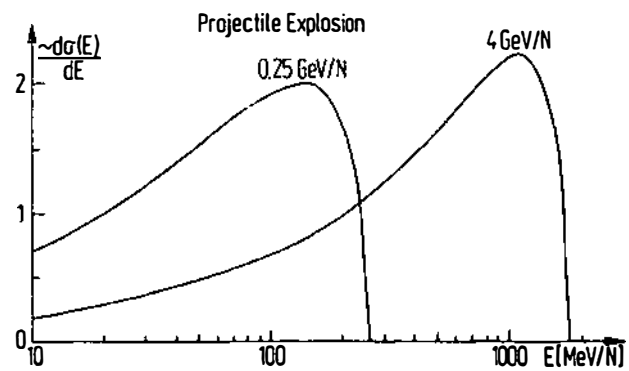

Fig. 16: The energy spectrum of the projectile, which explodes because of its high excitation energy when it leaves the target, is shown for E_{LAB}/N = 0.25 and 4 GeV/N.

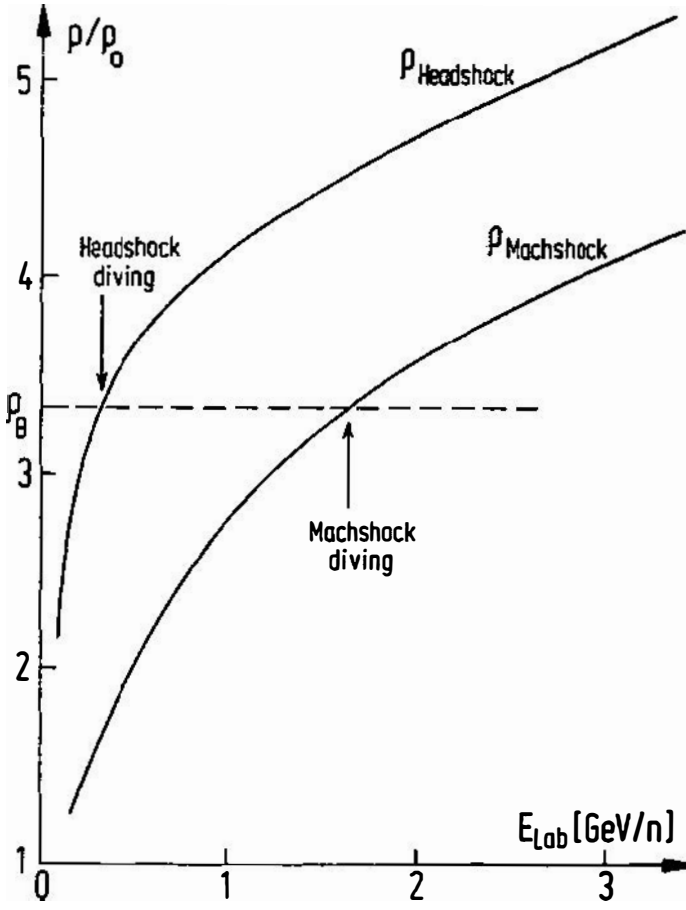

Fig. 17: The mean density in the head- and Mach shock respectively as function of the bombarding energy is depicted. A possible phase transition will effect the head shock at rather small energies, while the Mach shock will be effected only at much higher bombarding energies.

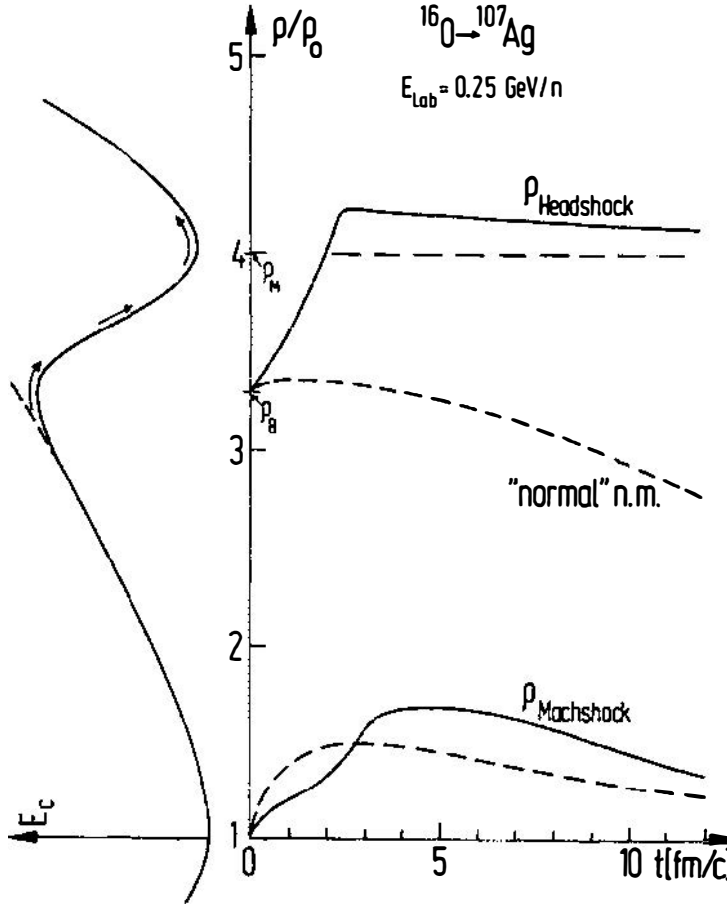

Fig. 18: shows the drastic consequences of a secondary minimum in $E_c(\rho)$ on the reaction: The head- and Mach shock density as a function of time is shown for two different $E_c(\rho)$: the dashed curves indicate normal nuclear matter, while the solid curves represent the results calculated with a phase transition at densities between 3.3 and 4 ρ_o: The headshock dives into the secondary minimum, which results in a smaller Mach shock angle (as described in the text). The lowering of the Mach shock angle can be used to determine the width of the region of negative pressure[43]: strong deviations of the Mach angle indicate large spreading of this phase transition region.

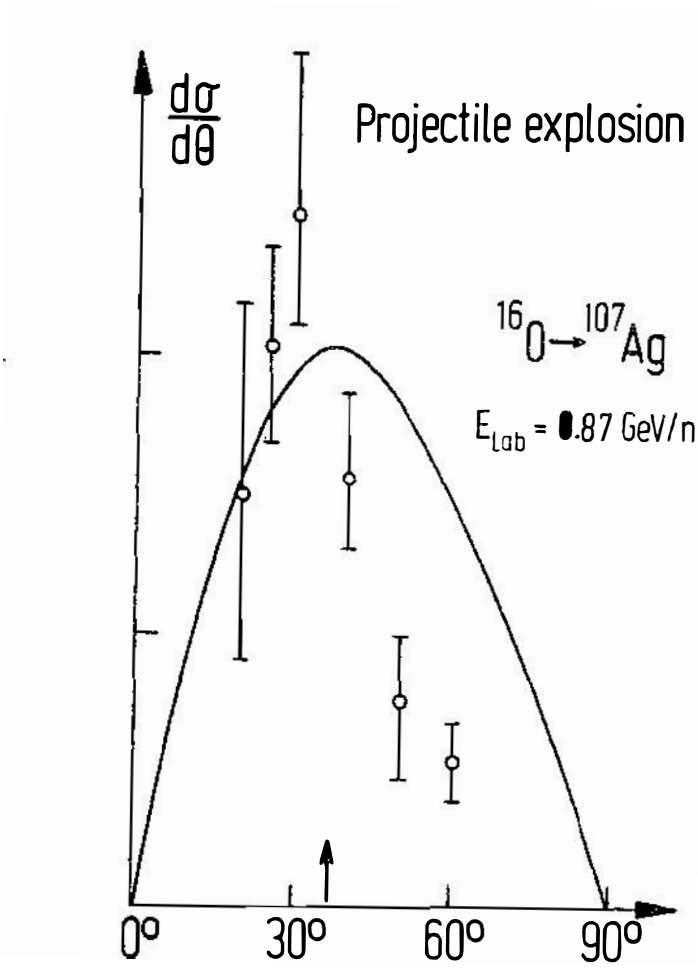

Fig. 19: The calculated angular distribution of the head shock particles (full curve) is compared to the result of a recent experiment[44] (dots; 0.8 GeV/n Ne→Pb): At least five fast (E_{LAB}> 200 MeV) azimuthally symmetric distributed protons have been measured in coincidence, which seems to indicate the existence of a rather compact highly excited projectile (head shock).

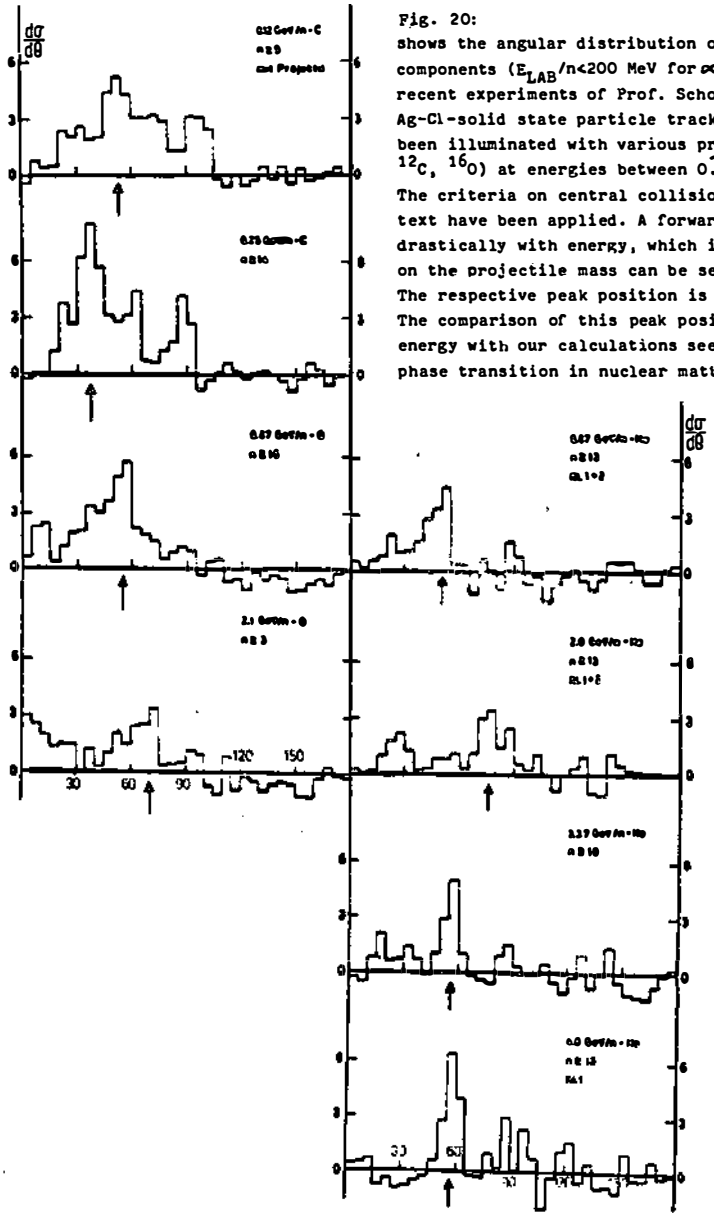

Fig. 20:
shows the angular distribution of the "no evaporation" components ($E_{LAB}/n<200$ MeV for α-particles) in the recent experiments of Prof. Schopper and coworkers.[40] Ag-Cl-solid state particle track detectors have been illuminated with various projectiles (^4He, ^{12}C, ^{16}O) at energies between 0.1 and 4.0 GeV/n. The criteria on central collisions as quoted in the text have been applied. A forward peak, shifting drastically with energy, which is nearly independent on the projectile mass can be seen.
The respective peak position is indicated by arrows. The comparison of this peak position as function of energy with our calculations seems to indicate a phase transition in nuclear matter at $\rho/\rho \approx 3$.